Journal of Structural Geology 32 (2010) 202–215

Contents lists available at ScienceDirect

Journal of Structural Geology

journal homepage: www.elsevier.com/locate/jsg

Static recrystallization of vein quartz pebbles in a high-pressure – low-temperature metamorphic conglomerate

Claudia Trepmann*, Annette Lenze, Bernhard Stöckhert

Institut für Geologie, Mineralogie und Geophysik, Ruhr-Universität Bochum, Sonderforschungsbereich 526, Germany

ARTICLE INFO

Article history:
Received 6 April 2009
Received in revised form
11 November 2009
Accepted 15 November 2009
Available online 23 November 2009

Keywords:
Quartz
Static recrystallization
Strain-induced grain boundary migration
Recovery
Fluid inclusions

ABSTRACT

Microfabrics of quartz pebbles in HP-LT (c. 1 GPa, c. 350 °C) metamorphic conglomerates are investigated. The conglomerate was deformed by dissolution-precipitation creep, while the interior of the pebbles remained undeformed. The different pebbles display a wide variety of quartz microstructures imported from the source rocks. One type of pebble is derived from quartz veins; it shows old grains with numerous fluid inclusions, subgrains, and undulatory extinction, which are partly replaced by new grains devoid of inclusions and substructure. Free dislocation densities are on the order of 10^{12} m^{-2} in both grains. We conclude that: (1) the quartz vein underwent inhomogeneous crystal-plastic deformation in the source rock; (2) recrystallization took place by strain-induced grain boundary migration starting from small crystalline volumes poor in defects; (3) recrystallization was purely static and commenced during re-burial of the conglomerate; which (4) was simultaneously deformed by dissolution-precipitation creep at low differential stress, insufficient for crystal-plastic deformation of quartz; (5) fluid inclusions within old grains were eliminated and their fluid content was drained along the migrating high angle grain boundaries; and (6) strain-induced grain boundary migration ceased once the driving force became too low by static recovery (concurrent to recrystallization) within the deformed old grains.

1. Introduction

Recrystallization is the migration and/or formation of high angle grain boundaries driven by the reduction of stored strain energy (White, 1977; Haessner and Hofmann, 1978; Vernon, 1981; Jessell, 1986; Urai et al., 1986; Drury and Urai, 1990). Recrystallization is a thermally activated process. Thus, it requires sufficient temperatures, usually above a homologous temperature T/T_m of about 0.4 (T_m denoting the absolute melting temperature of the material).

Recrystallization can be dynamic or static. Dynamic recrystallization occurs contemporaneous with deformation, in the regime of dislocation creep. Static recrystallization occurs without deformation in the absence of differential stress. It reduces the stored strain energy in a material that has acquired a high dislocation density during a preceding stage of glide-controlled crystal-plastic deformation at lower temperatures and higher stress in the low-temperature plasticity regime, where recovery and recrystallization are not effective. Dynamic recrystallization is common in merely all earth materials deforming by creep at elevated temperatures (T/T_m above about 0.4) and at moderate to high-stress in the deeper crust and mantle, as demonstrated by the microstructure of exhumed metamorphic rocks. In contrast, static recrystallization is less commonly reported for natural earth materials. Here, the term static is taken to mean recrystallization without notable contemporaneous crystal-plastic deformation, hence at very low differential stress. Strictly speaking, the process should be termed quasi-static, as an environment where differential stress is approaching zero is probably a very rare exception in the interior of the earth.

Four different geological scenarios leading to static recrystallization can be envisaged. Each involves a preceding stage of crystal-plastic deformation at low-temperature and/or high strain rate.

(A) A rock, where minerals had undergone glide-controlled plastic deformation at high differential stress in the upper crust, is progressively buried and finally enters a very low-stress environment with higher temperatures at greater depth. The relevance of scenario (A) in nature is difficult to assess: firstly, a tectonic situation where a rock is plastically deformed at moderate temperatures in the upper crust and then enters a nearly stress-free environment, when buried into the deeper crust by active tectonics, is not very likely. Active tectonics can be expected to cause deformation by dislocation creep accompanied by dynamic recrystallization in a deeper crustal level. Secondly, microstructures developing during progressive burial would readily be overprinted during exhumation by a sequence of processes commonly including high-stress

* Corresponding author. Tel.: +49 234 322 7765; fax: +49 234 321 4572.
E-mail addresses: claudia.trepmann@rub.de (C. Trepmann), annette.lenze@rub.de (A. Lenze), bernhard.stoeckhert@rub.de (B. Stöckhert).

0191-8141/$ – see front matter © 2009 Elsevier Ltd. All rights reserved.
doi:10.1016/j.jsg.2009.11.005

deformation at the crustal scale brittle-ductile transition horizon. This leaves little potential for identification of an early stage of static recrystallization during burial.

(B) A rock, whose minerals had undergone some crystal-plastic deformation during a preceding stage of the tectonic history, is heated by intruding magma in the upper crust, which leads to stress relaxation on a regional scale and annealing processes on the microscale. This scenario may be common wherever large magma bodies intrude the upper crust in a tectonically calm environment, for instance in regions of intraplate hot spot magmatism. In this case, the intracrystalline strain energy has been acquired when the host rock passed upwards earlier through the crustal scale brittle-ductile transition horizon, for which the highest stress levels in the Earth's interior are expected. Afterwards the temperatures were too low to drive thermally activated processes, until heating of the cool upper crust by intruding magma. The general validity of scenario (B) is supported by observations indicating static recrystallization and grain growth in contact aureoles surrounding plutons with a shallow level of emplacement (e.g. Buntebarth and Voll, 1991; Wirth, 1985; Piazolo et al., 2005; Otani and Wallis, 2006).

(C) Instantaneous loading related to stress redistribution during seismogenic faulting causes glide-controlled crystal-plastic deformation, commonly localized along fractures and in small-scale plastic shear zones (Trepmann et al., 2007). This can take place at elevated temperatures in the middle or deeper crust (Trepmann and Stöckhert, 2003; Nüchter and Stöckhert, 2008; Birtel and Stöckhert, 2008). When the period of stress relaxation is short, quasi-static recrystallization restricted to the damaged crystal volume can take place (Trepmann et al., 2007). This scenario is probably common in the middle crust of tectonically active regions, at temperatures where the material undergoes viscous deformation by dislocation creep at a long term, but is strongly affected by stress redistribution during major seismogenic faulting in the overlying upper crust (Trepmann et al., 2007).

(D) Erosion of rocks, whose minerals were plastically deformed at high-stresses and decreasing temperatures during the preceding exhumation, yields clastic grains with a high dislocation density into a sedimentary basin. When this sedimentary rock is buried and heated during basin subsidence (case D_1), or incorporated into an accretionary complex deforming at very low-stress by dissolution-precipitation creep (case D_2), static recrystallization is possible. Both scenarios are probably common, though – to our knowledge – not extensively reported so far. The first case (D_1) may be widespread in deep sedimentary basins and at passive continental margins, where burial and diagenesis of sediments takes place without pervasive tectonic deformation and where the stress field is governed by overburden load. In principle, the situation could directly be observed in samples from the bottom part of the deepest gas wells, depending on the local geotherm. Observation of microstructures indicating static recrystallization in clastic quartz particles within the sedimentary rock may be valuable for the reconstruction of the thermal history.

The record of the second case (D_2) is potentially accessible in exhumed accretionary prisms (e.g. Platt, 1986, 1993; Ring et al., 1999) and shallow portions of subduction channels (e.g. Gerya et al., 2002; Gerya and Stöckhert, 2006; Bachmann et al., 2009). As in the case of pure subsidence and burial by younger sediments, pore fluid pressure is expected to reach near-lithostatic values at shallow depths of a few kilometres, tectonic deformation of clastic sediments being then probably governed by dissolution-precipitation creep at very low differential stress (e.g. Schwarz and Stöckhert, 1996; Stöckhert et al., 1999). Many rocks buried to and exhumed from depths of several tens of kilometres show no sign of crystal-plastic deformation during that part of their history (Stöckhert, 2002).

In both cases outlined as scenario (D), the microfabrics of clastic minerals acquired by deformation during exhumation and cooling in their source area can be modified by static recrystallization at low differential stress. The driving force is the stored intracrystalline strain energy, bound to a high dislocation density, which is brought into the sediment. Heat input concomitant with burial in a low-stress environment, where bulk deformation or compaction of the rock is governed by dissolution-precipitation creep, then leads to release of the internal stored strain energy by static recrystallization, without renewed crystal-plastic deformation.

Here we analyze an example, corresponding to scenario (D_2), where clastic quartz grains plastically deformed in their source rock were heated to moderate temperatures in a low-stress environment at a convergent margin.

2. Geological setting and sample location

The Island of Crete is a horst structure in the forearc area of the Hellenic subduction zone located within the eastern Mediterranean Sea (Fig. 1). The internal structure of the island is characterized by tectonic nappes that originated during northward subduction of oceanic crust and subsequent collision of the northern margin of a microcontinent belonging to the African Plate with the southern margin of the Eurasian Plate in mid-Miocene times (Kilias et al., 1994; Fassoulas et al., 1994; Jolivet et al., 1996; Thomson et al., 1998, 1999). Parts of the sedimentary cover of the microcontinent underwent HP-LT metamorphism during collision. They were rapidly exhumed, interpreted to be a consequence of roll back (Thomson et al., 1998, 1999; Seidel et al., 2007). The nappe pile is divided into two groups: the lower group is composed of the Plattenkalk and the Phyllite-Quartzite units, which show pervasive Oligocene–Miocene HP-LT metamorphism (Seidel et al., 1982; Theye, 1988; Theye and Seidel, 1991; Theye et al., 1992), whereas the units of the upper group do not show evidence of Tertiary metamorphism or at best very low-grade metamorphism (Rahl et al., 2005). In central Crete, the HP-LT metamorphic rocks are exposed in the Talea and the Psiloritis windows (e.g., Theye, 1988; Theye et al., 1992; Kilias et al., 1994; Jolivet et al., 1996; Chatzaras et al., 2006).

The Plattenkalk (German for platy limestone) unit represents the lowermost exposed unit of the nappe pile. It comprises an Upper Carboniferous to Eocene sequence of carbonate rocks (König and Kuss, 1980; Richter and Kopp, 1983; Krahl et al., 1988; Chatzaras et al., 2006). The lowermost parts of the Plattenkalk unit are only known from the Talea Ori area in central Crete (Epting et al., 1972; Hall and Audley-Charles, 1983; Seidel et al., 1982; Richter and Kopp, 1983). There, quartz conglomerates are interpreted as the Permian base of the Plattenkalk unit (König and Kuss, 1980). The base of these conglomerates is not identified. The conglomerates are overlain by the Permian Galinos slates, the Upper Carboniferous to Upper Triassic Fodele and Sisses beds, and an Upper Triassic to Lower Jurassic stromatolitic dolomite marble (Epting et al., 1972; König and Kuss, 1980). Jurassic to Eocene marbles form the Plattenkalk sensu stricto overlain by Oligocene flysch deposits on the very top (Epting et al., 1972). Metamorphic index minerals (magnesiocarpholite, pyrophyllite, diaspore, sudoite) have been found in metamorphic bauxites within the Plattenkalk unit of the Talea Ori window, indicating P-T conditions of c. 1 GPa at c. 350 °C (Seidel et al., 1982; Theye, 1988; Theye et al., 1992).

The Plattenkalk unit is overthrust by the Phyllite-Quartzite unit, which represents an Upper Carboniferous to Triassic metasedimentary rift sequence (Krahl et al., 1988). It shows widespread evidence of HP-LT metamorphism at conditions of $T = 400 \pm 50$ °C and $P \approx 1$ GPa in western Crete, both T and P gradually decreasing eastwards (Theye and Seidel, 1991; Brix et al., 2002). The age of this metamorphism is constrained at c. 24 Ma by K–Ar and Ar–Ar ages

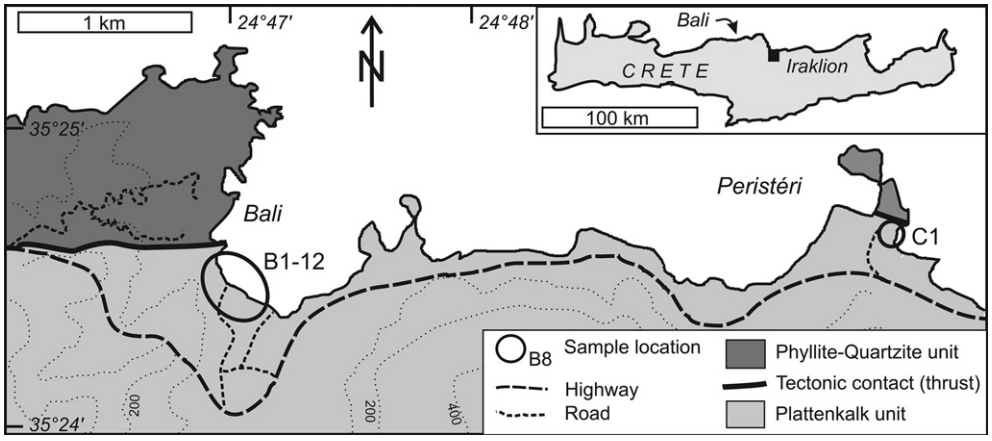

Fig. 1. Sample locations at the northern coast of Crete, about 50 km west of Iraklion.

of white mica from the Phyllite-Quartzite unit (Seidel et al., 1982; Jolivet et al., 1996). Combined fluid inclusion (Küster and Stöckhert, 1997) and fission-track data of zircon and apatite (Thomson et al., 1998, 1999) from the Phyllite-Quartzite unit indicate that subsequent exhumation to a depth of about 10 km and cooling to about 300 °C was completed by 19 Ma and final cooling to about 100 °C took place at about 15 Ma.

The microstructures observed in the Phyllite-Quartzite unit reflect deformation by dissolution-precipitation creep under low differential stress and near-lithostatic pore fluid pressure at maximum depth of burial. This pervasive deformation is attributed to detachment from the downgoing plate (Schwarz and Stöckhert, 1996; Stöckhert et al., 1999). In contrast, no pervasive deformation is recorded for the subsequent stage of rapid exhumation, before the Phyllite-Quartzite unit became part of the brittle upper crust (Thomson et al., 1999). A similar history seems likely for the Plattenkalk unit, where fossil shells are preserved entirely undistorted (Epting et al., 1972; König and Kuss, 1980) and palisade structures of calcite presumably grown at the expense of aragonite (as described from Syros by Brady et al., 2004) are locally observed. This structural record is regarded as analogous to that of undeformed though ultrahigh pressure metamorphic granites (Biino and Compagnoni, 1992; Renner et al., 2001; Lenze and Stöckhert, 2007), and coarse undeformed palisade structures of quartz grown at the expense of coesite in the rock matrix during exhumation (e.g. Schertel et al., 1991; Lenze and Stöckhert, 2008), both observed in the UHP metamorphic Dora Maira massif, western Alps.

The outcrops of the investigated quartz conglomerate are located at the Permian base of the Plattenkalk unit (Epting et al., 1972; König and Kuss, 1980) in the Talea Ori window at the northern coast of Crete, about 53 km west of Iraklion, near the village of Bali (Fig. 1). Samples were taken at two sites, labelled C1 (35°24′38″N, 24°49′38″E) and B1–B12 (35°24′39″N, 24°46′57″E–35°24′30″N–24°47′00″E) on the map in Fig. 1.

3. Methods

The microstructures of the conglomerate were examined in polished thin sections (~30 μm) with a polarising microscope. The crystallographic orientation and microfabric of quartz was analysed by scanning electron microscopy (SEM), using a LEO 1530 instrument with field emission gun, forescatter detector and electron backscatter diffraction (EBSD) facilities. The SEM was operated at an accelerating voltage of 20 kV, with the thin section tilted at an angle of 70° with respect to the beam, and with a working distance of 25 mm. For automatic indexing and processing of the data, the HKL *CHANNEL5* software was used. Patterns indexed with a mean angular deviation (MAD) of >1.0 have been excluded during data collection. Further processing included the automatic removal of incorrectly indexed isolated points and the replacement of non-indexed points by the most common orientation of a specified number (6–7) of neighbouring indexed points. The original percentage of points indexed as quartz was 50–83%. Processing of the raw data results in an improved indexing percentage of 60–92%. For the analysis of grain parameters, a misorientation angle of more than 10° was taken to represent a high angle grain boundary (White, 1977). The specific misorientation relation given by a rotation of $60 \pm 5°$ around [001] was taken to represent a Dauphiné twin boundary. Because of the widespread occurrence of Dauphiné twins, especially in old grains, the angles between *c*-axes of old and new grains are displayed in addition to the misorientation angle.

TEM samples covering the boundaries between recrystallized and old quartz grains were prepared by the focussed ion beam (FIB) technique using a FEI Quanta200 3D instrument. This technique allows the preparation of site-specific electron transparent foils (10–20 μm wide, 5–15 μm high and 100–200 nm thick) by Ga-ion milling from a standard thin section (Wirth, 2004), with the ability to maintain perfect spatial correlation between optical and TEM features. The TEM samples are prepared as slices perpendicular to the plane of the thin section. As an artefact introduced by FIB preparation, TEM samples show fissures at their bottom edge, which may be related to bends in steeply inclined grain boundaries. In TEM samples without steeply inclined grain boundaries this effect has not been observed. To investigate the intracrystalline substructure of deformed host grains, TEM samples were prepared by conventional ion milling (GATAN PIPS). Both kinds of TEM samples were examined with a Philips EM301 transmission electron microscope operated at 100 kV. All diffraction contrast images were produced using bright field (BF) conditions. Dislocation densities ρ were estimated from TEM micrographs by counting the number of dislocation lines (N) intersecting a unit area (A) with $\rho = 2N/A$ (Karato, 2008).

4. The Bali quartz conglomerate

The Bali conglomerate is conspicuous in outcrop due to the black colour of the majority of the quartz pebbles. The pebbles are well-rounded, more or less ellipsoidal in shape, with the long axis measuring several millimetres to some centimetres (Fig. 2). The aspect ratio in 2D-sections perpendicular to foliation and parallel to lineation ranges between 1 and 5, with a typical value of about 2. Besides the predominating quartz pebbles, other rock types occur

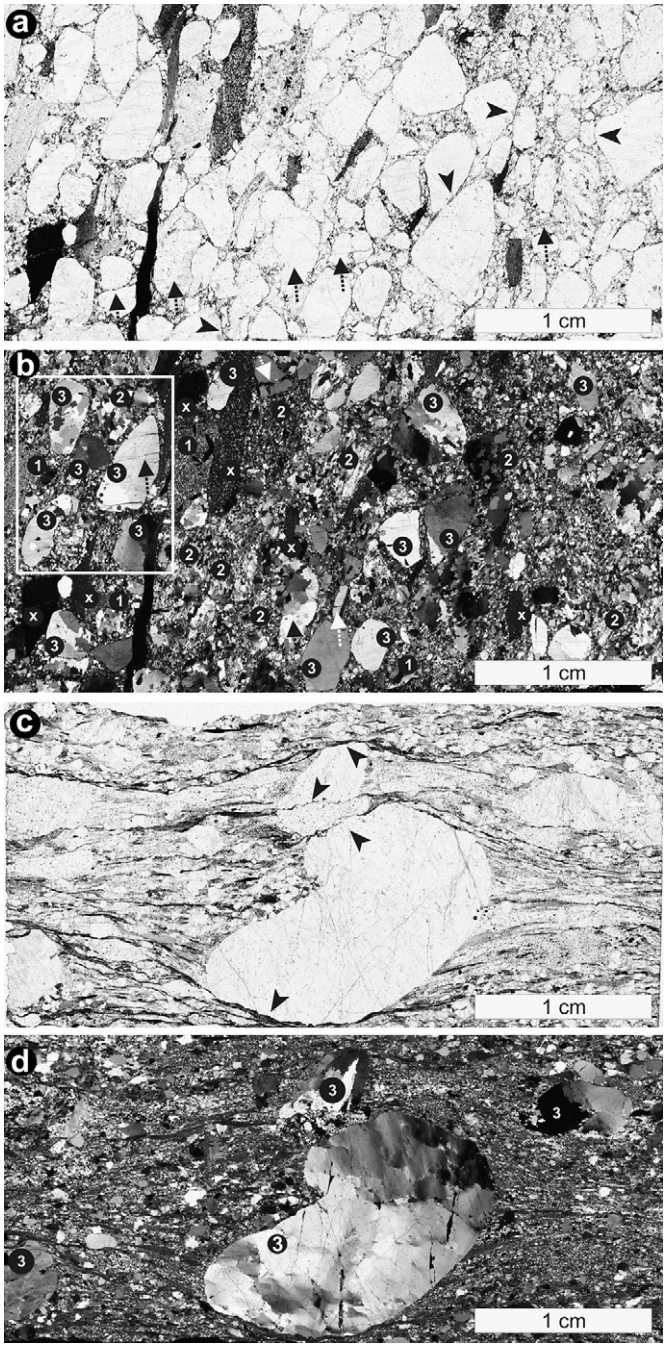

Fig. 2. Optical micrographs of the Bali conglomerate: (a) sample B8 is showing well-rounded, approximately ellipsoidal pebbles. The pebbles show indented contacts, with passive enrichment of less soluble mica (black arrows). Dashed arrows point to a fracture continuing through several pebbles. (b) Micrograph taken with crossed polarizers of same sample as shown in (a). The pebbles are labelled according to the different types of source rock (*x*, 1–3), see text for discussion. The white rectangle represents area displayed in Fig. 3a. (c) Sample B7 shows a foliation in the matrix defined by the SPO of mica and quartz. The pebbles show indented contacts, with passive enrichment of less soluble mica (black arrows). (d) Micrograph taken with crossed polarizers of the same sample as shown in (c).

in minor proportions, including impure cherts, slates, schists, and rarely gneisses (labelled "*x*" in Fig. 2). Calcite veins occur in places.

The quartz pebbles are classified into three major types according to their microstructure. The relative proportions of the three types in the different samples are highly variable (Fig. 2). Type 1 quartz pebbles contain mica and show a shape preferred orientation (SPO). These pebbles are derived from low-grade metamorphic impure sandstones. Type 2 pebbles are composed of almost pure quartz aggregates. They show sutured high angle grain boundaries (HAGBs) and a more or less pronounced crystallographic and shape preferred orientation; some display a foam structure. These pebbles are derived from pure silicic metasediments or deformed and completely recrystallized quartz veins. Type 3 pebbles comprise few (typically 1–3) large quartz grains with numerous fluid inclusions, undulatory extinction and subgrains; some of the latter show relics of fibrous grain shape typical for vein quartz grown by the crack seal mechanism (Durney and Ramsay, 1973). These pebbles are derived from a broad variety of quartz veins within the source area. In many of the type 3 pebbles, new quartz grains devoid of fluid inclusions, undulatory extinction and subgrains have grown at the expense of the original deformed vein quartz.

The matrix of the conglomerate is mainly composed of fine-grained quartz, white mica, iron oxyhydrates, opaque minerals, chlorite, stilpnomelane, chlorite, tourmaline, and occasionally feldspar (Fig. 2). The SPO of mica and quartz in the matrix, as well as the preferred orientation of the long axis of the pebbles, define the more or less obvious foliation and stretching lineation (Fig. 2). For pebbles with an anisotropy inherited from the source area (type 1 quartz pebbles and pebbles that were derived from cherts, slates, schists, and gneisses). This internal foliation tends to be at a low angle to the foliation of the conglomerate (Figs. 2b,d), but considerable deviation occurs (Fig. 2) and marked deviation between neighbouring pebbles is obvious. Pebbles show indented particle contacts, stylolites, strain caps with enrichment of insoluble minerals (black arrows in Figs. 2a,c), and strain shadows. In places, healed fractures in the conglomerate can be traced through several of the pebbles and occur at an angle of 70–80° to the foliation (dashed arrows in Fig. 2a). Such continuous fractures are locally overgrown by the new recrystallized grains in type 3 pebbles (dashed arrows in Figs. 2a,b and 3a,b).

The focus of this study is the microfabric of the type 3 quartz pebbles and the formation of the new grains.

5. Microfabric of the type 3 quartz pebbles

The deformed vein quartz in type 3 pebbles appears dusty in transmitted light due to a high content of fluid inclusions mostly aligned in trails (Figs. 3 and 4) defining healed microcracks. These old grains show a marked undulatory extinction and subgrains of variable size. The "dusty" appearance of these old grains is in marked contrast to the "clear" appearance of new grains devoid of fluid inclusions, undulatory extinction and subgrains. The proportions of the undeformed new and deformed old grains are variable (Figs. 3 and 4). The boundaries between new and old grains are highly sutured and extensively bulge into the old grain (white arrows in Figs. 3a and 4a–c). In contrast, high angle grain boundaries (HAGBs) separating two new grains are planar or slightly curved (black arrows in Figs. 4b,c). Locally, HAGBs between three new grains exhibit equilibrium angles of 120° (black arrow in Fig. 4d). Along HAGBs between old grains, low angle grain boundaries (LAGBs) defining subgrains are particularly widespread (black arrows in Figs. 4e,f). LAGBs are very rarely observed in new grains.

The internal variation of the *c*-axis orientation within individual old grains, which reflects the density of geometrically necessary dislocations introduced during inhomogeneous crystal-plastic deformation, reaches 15° (Figs. 5c and 6c). In contrast, new grains devoid of an optically visible substructure show a very low variation in *c*-axis orientation, mostly markedly smaller than 3°, as displayed by the small circles in Figs. 5d and 6d. Dauphiné twins with irregular boundaries are common in old grains (yellow lines in Figs. 5a and 6a). In new grains they are rare and show planar boundaries (Fig. 5a).

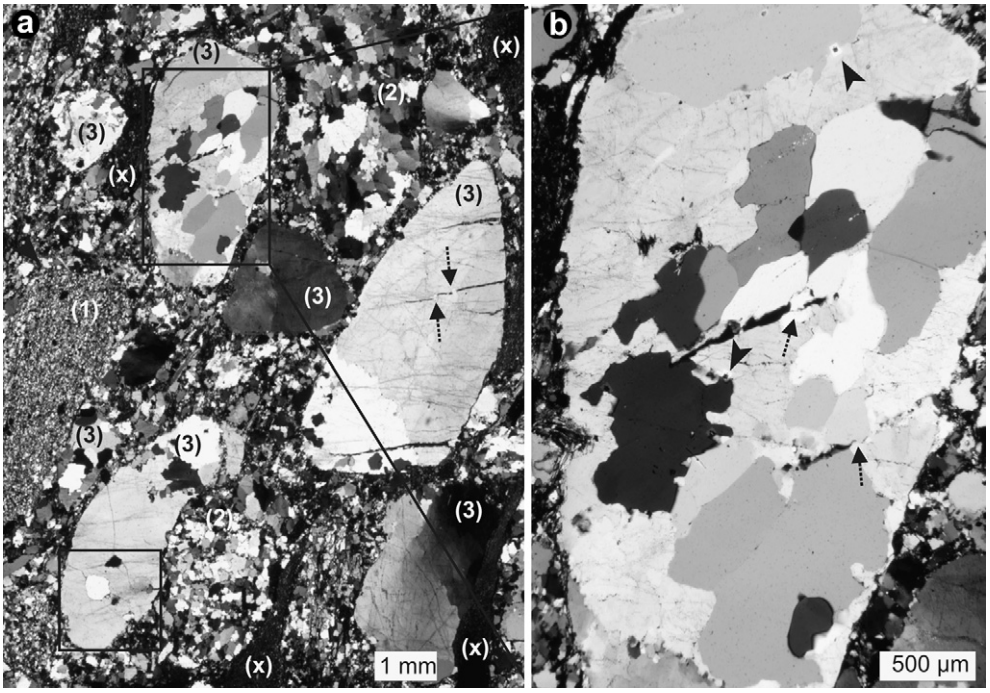

Fig. 3. Optical micrographs showing the quartz microstructure in type 3 pebbles; crossed polarizers, sample B8. (a) The pebbles are labelled according to the different types of source rocks (*x*, 1–3), see text for discussion. In places, new grains overgrow fractures that continue through several adjacent pebbles (dashed arrows). The upper right rectangle shows the pebble displayed in (b). An EBSD map of this pebble is presented in Fig. 5, and an enlarged one of the area marked by the lower left rectangle in Fig. 6. (b) Type 3 quartz pebble is composed of deformed old grains and clear new grains. New grains overgrow fractures that can be traced through several adjacent pebbles (dashed arrows). Solid arrows point to the FIB-cuts, from which the TEM-images presented in Figs. 8 and 9 were taken.

The crystallographic misorientation between old and new grains is ranging between 12° and 90° and the average is 68° (Figs. 5b and 6b). The angle between *c*-axes of new and old grains is on average 52°, ranging from 7 to 90° (Figs. 5c,d and 6c,d). There is no systematic crystallographic orientation relation between old and new grains (Figs. 5c,d and 6c,d).

TEM observations reveal that the free dislocation density is generally low in both old (Fig. 7) and new grains (Figs. 8 and 9). In the old grains it appears to be at best slightly higher (about 10^{12} m^{-2}) compared to new grains (about $5 * 10^{11}$ m^{-2}). The LAGBs in old grains are generally well-ordered (Figs. 7c–f) and can be weekly lobate (black arrows in Fig. 7d). Gently curved or planar LAGBs define isometric subgrains (Fig. 7e). Three LAGBs can meet at 120° angles (Figs. 7e,f). Small fluid inclusions in old grains are frequently linked to LAGBs (black arrows in Figs. 7d and 8c–d). No LAGBs and no fluid inclusions are observed in the new grains using TEM (Figs. 8 and 9). The boundaries between old and new grains do not follow crystallographic planes (Figs. 8 and 9). They truncate the LAGBs in old grains with dihedral angles slightly below 180° due to the low interfacial free energy of the LAGBs (white arrows in Figs. 8c–f,h). In contrast, they are straight where the old grain is devoid of LAGBs (Figs. 9c–f,h). The boundaries between old and news grains are frequently decorated by voids showing a dihedral angle well below 60° (black arrows in Figs. 8f and 9e,f).

6. Discussion

6.1. Deformation of the conglomerate

The conglomerate was deformed by dissolution-precipitation creep, as demonstrated by indented particle contacts, stylolites, strain caps with insoluble minerals enriched (black arrows in Figs. 2a,c), and strain shadows. The unsystematic orientation of the internal foliation in the pebbles in relation to the foliation of the conglomerate indicates that the pebbles had a primarily anisometric shape controlled by source rock anisotropy. The shape preferred orientation acquired with sedimentation was enhanced by dissolution-precipitation creep in the conglomerate. The wide variety of microstructures and the variable orientation of the internal fabrics suggest that the quartz pebbles remained internally undeformed.

Healed fractures can be traced through adjacent pebbles (dashed arrows in Figs. 2a,b), precluding their formation in the source area. Instead, these fractures must have formed in the present assembly of the conglomerate.

6.2. Microfabric development in the type 3 quartz pebbles

6.2.1. Formation of new grains by static recrystallization

Type 3 pebbles are composed of: (1) large deformed old quartz grains showing subgrains, undulatory extinction and abundant fluid inclusions along healed microcracks; and (2) new grains devoid of fluid inclusions and internal substructure. The fact that new grains overgrow late fractures that formed in the conglomerate (dashed arrows in Figs. 3a,b) demonstrates that also the new grains must have grown within the conglomerate, and are not imported from the source rock. The strain-free new grains do not show a crystallographic preferred orientation or a specific orientation relation to the host grain (Figs. 5–7). These observations indicate that the growth of new grains has taken place within the conglomerate, long after the deformation of the old grains within the source rock, and at static conditions with negligible differential stress.

Static recrystallization involves the migration of a high angle boundary into the grain with the higher dislocation density (White, 1977; Haessner and Hofmann, 1978; Vernon, 1981; Poirier, 1985; Jessell, 1986; Urai et al., 1986; Knipe, 1989; Drury and Urai, 1990; Masuda et al., 1997; Humphreys and Hatherly, 2004; Passchier and Trouw, 2005), lowering the stored strain energy in the system. This

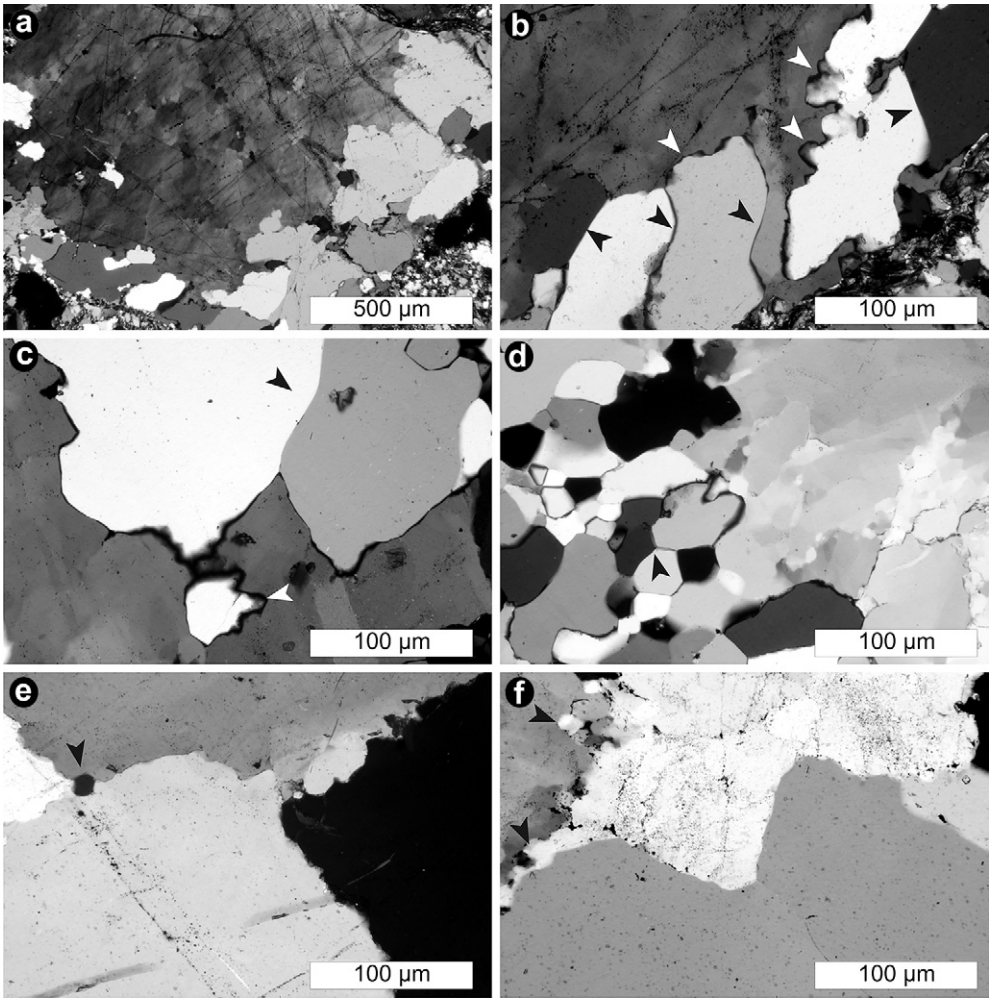

Fig. 4. Optical micrographs of old and new grains within type 3 quartz pebbles; crossed polarizers. (a) An old grain is showing strong undulatory extinction and fluid inclusions aligned along healed microcracks (sample C17). The old grain is surrounded by new grains. (b, c) The grain boundaries between old and new grains are irregular and strongly sutured (white arrows), whereas the boundaries between the new grains are straight or smoothly curved (black arrows; sample C17 and sample B12, respectively). (d) The boundaries of three new grains are enclosing an angle of 120° (black arrow). (e, f) The boundaries between two old grains are irregular and flanked by subgrains (white arrows; sample C17 and sample B8, respectively).

strain-induced grain boundary migration (SIGBM) leads to lobate boundaries (White, 1982; Urai et al., 1986; Drury and Urai, 1990), as observed in the type 3 pebbles (white arrows Figs. 4b,c). In experimentally deformed and annealed synthetic rocksalt, Bestmann et al. (2005) and Piazolo et al. (2006) differentiated between slow migration of boundaries between pre-existing old grains containing a substructure (GBM1) and rapid migration of boundaries between initially small grains without substructure and old deformed grains (GBM2). In the case of GBM2, new grains grow free of LAGBs, originating from small crystalline volumes devoid of geometrically necessary dislocations and LAGBs. In the case of GBM1, LAGBs are observed to continue into the recrystallized volume behind the migrated HAGB, consistent with the prerequisite that dislocations cannot end within a crystal. This has also been observed in naturally deformed and subsequently annealed quartz (Piazolo et al., 2005). Jessell et al. (2003) showed by comparison of microstructural simulations and natural microstructures in recrystallized peridotite that migration of boundaries between old grains can lead to "unswept" inclusion-rich cores and "swept" clear inclusion-free rims.

In the present case, the growth of new defect-poor grains by SIGBM at the expense of old deformed grains, corresponding to GBM2 (Piazolo et al., 2006), is evident from the microstructure. If the new crystalline volume had been created by the migration of long grain boundary segments between two old grains (GBM1; Bestmann et al., 2005), one would expect the new grains to contain abundant LAGBs. The process is referred to as "substructure drag" by Humphreys and Hatherly (2004). This is not observed; most new grains are entirely free of LAGBs. Also, a contrast in the concentration of fluid inclusions would be expected, i.e. clear rims surrounding cores rich in inclusions (Jessell et al., 2003); again, this is not the case. Instead, the large new grains are free of fluid inclusions (Figs. 4–6, 8 and 9).

At this point, the question concerning the origin of the new grain arises. It cannot be solved satisfactorily based on the available microstructural observations, as early stages of the microstructural history are routinely erased during the subsequent evolution. Furthermore, severe limitations are posed by the classical problem of stereology, i.e. the exclusive use of a 2D-section through a 3D-structure, and the inferred small size of the defect-free crystal volume that grew to large new grains in three dimensions.

Two possibilities for the origin of the new grains are envisaged in these rocks:

(1) The new grains have grown by SIGBM from single subgrains developed along HAGBs between two old grains (Figs. 4e,f). Such subgrains can readily grow into the neighbouring deformed grain

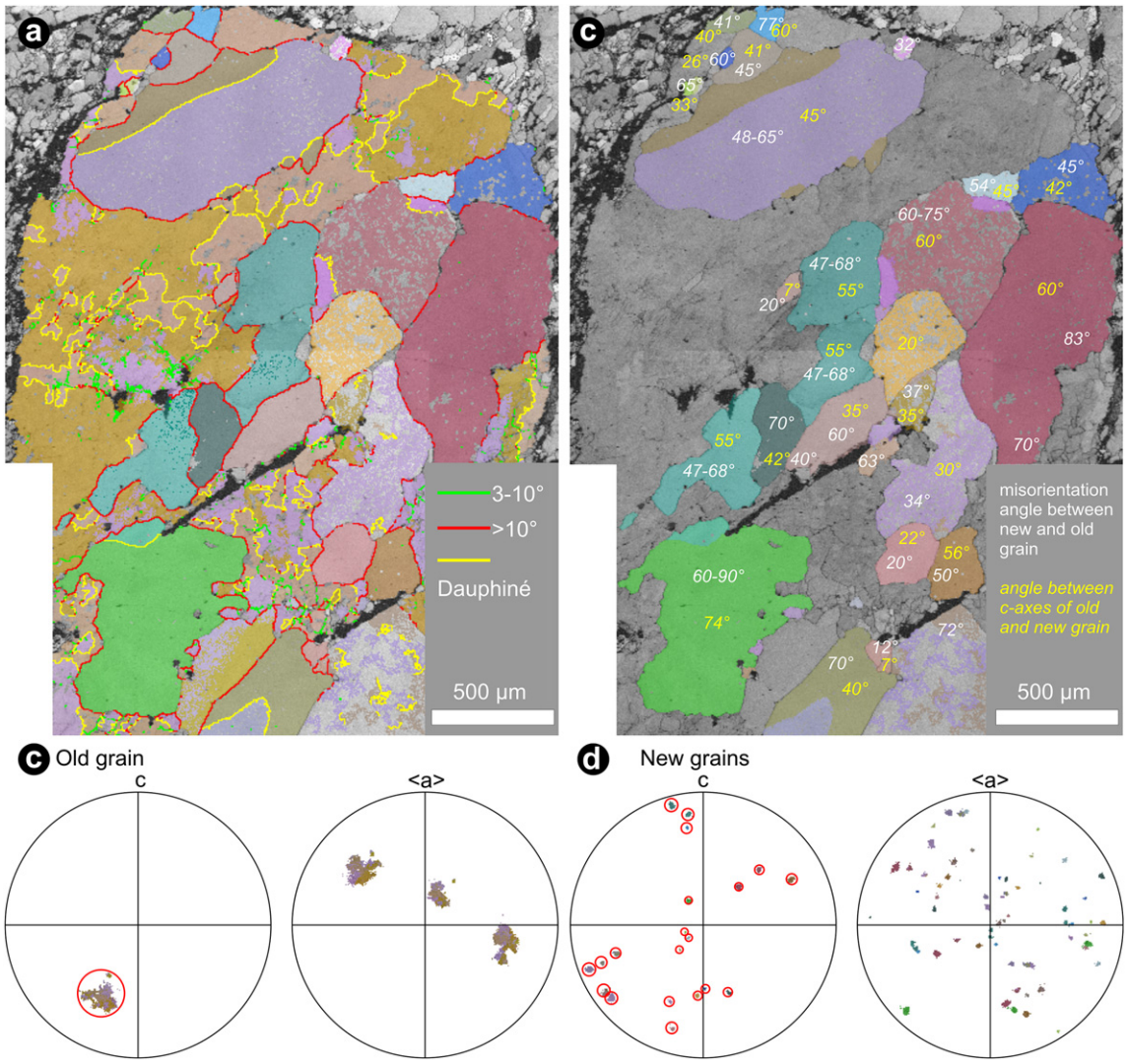

Fig. 5. EBSD map of quartz pebble shown in Fig. 3a (upper right rectangle, sample B8, step size 5 µm). (a) Orientation map of the quartz pebble; the surrounding matrix is displayed by band contrast only. Green lines represent LAGBs with misorientation angles of 3–10°, red lines represent HAGBs with misorientation angles >10°; Dauphiné twin boundaries are displayed by yellow lines. (b) The crystallographic orientations of new grains are colour coded, whereas the old grain and the matrix are displayed by band contrast only. The numbers represent the misorientation angles between new and old grain. (c, d) Pole figures (equal angle, lower hemisphere) of *c*- and ⟨*a*⟩ axes of new grains and old grain, respectively. The red small circles visualize the variations of the *c*-axis orientations of <15° for the old grain and <3° for new grains.

by bulging of the HAGB (Humphreys and Hatherly, 2004). New grains formed during annealing at the expense of a deformed host grain have been observed to show similar orientations as the old grain (Hobbs, 1968). In the type 3 quartz pebbles, however, a considerable number of new grains grew with crystallographic orientations markedly different from that of the host grain (Figs. 2, 5 and 6). At static conditions, additional subgrain rotation (Fitz-Gerald et al., 1983; White and Mawer, 1988; Stipp et al., 2002; Stipp and Kunze, 2008) can hardly account for the observed diversity of orientations. Therefore, this possibility appears less likely.

(2) The new grains have grown by rapid SIGBM from small, defect-poor, and randomly oriented crystallites pre-existent in the deformed microstructure. In this process, grains with a higher misorientation are favoured because of the higher mobility of high angle grain boundaries (e.g. Haessner and Hofmann, 1978, Piazolo et al., 2006; Stöckhert and Duyster, 1999). This possibility is supported by the observed diversity of orientations of new grains, given the fact that there are only few original vein quartz orientations in a single pebble (Figs. 5 and 6). In view of the intense crystal-plastic deformation of the vein quartz in type 3 pebbles, these small defect-free crystals with sufficient misorientation could have been formed along microcracks or zones of intense localized plastic deformation. From laboratory experiments, in which inhomogeneous deformation at high-stress was followed by static annealing, Trepmann et al. (2007) reported localized static recrystallization starting from small defect-poor crystallites. These crystallites were formed at small-scale plastic shear zones and in the damage zone of microcracks by a yet unspecified process. An identical microstructural record was also observed in naturally deformed vein quartz (Trepmann et al., 2007). Notably, the recrystallized grains do not exhibit a specific crystallographic relation to the host grain and are restricted to the region of highly localized deformation and damage.

6.2.2. Recovery

During post-deformational annealing, the stored strain energy is reduced by two concurrent processes: recovery and recrystallization (e.g. Guillopé and Poirier, 1979; Poirier and Guillopé, 1979; Poirier, 1985; Urai et al., 1986; Drury and Urai, 1990). The process of recovery involves intracrystalline reorganization of defects such as annihilation of dislocations of opposite sign and a re-configuration

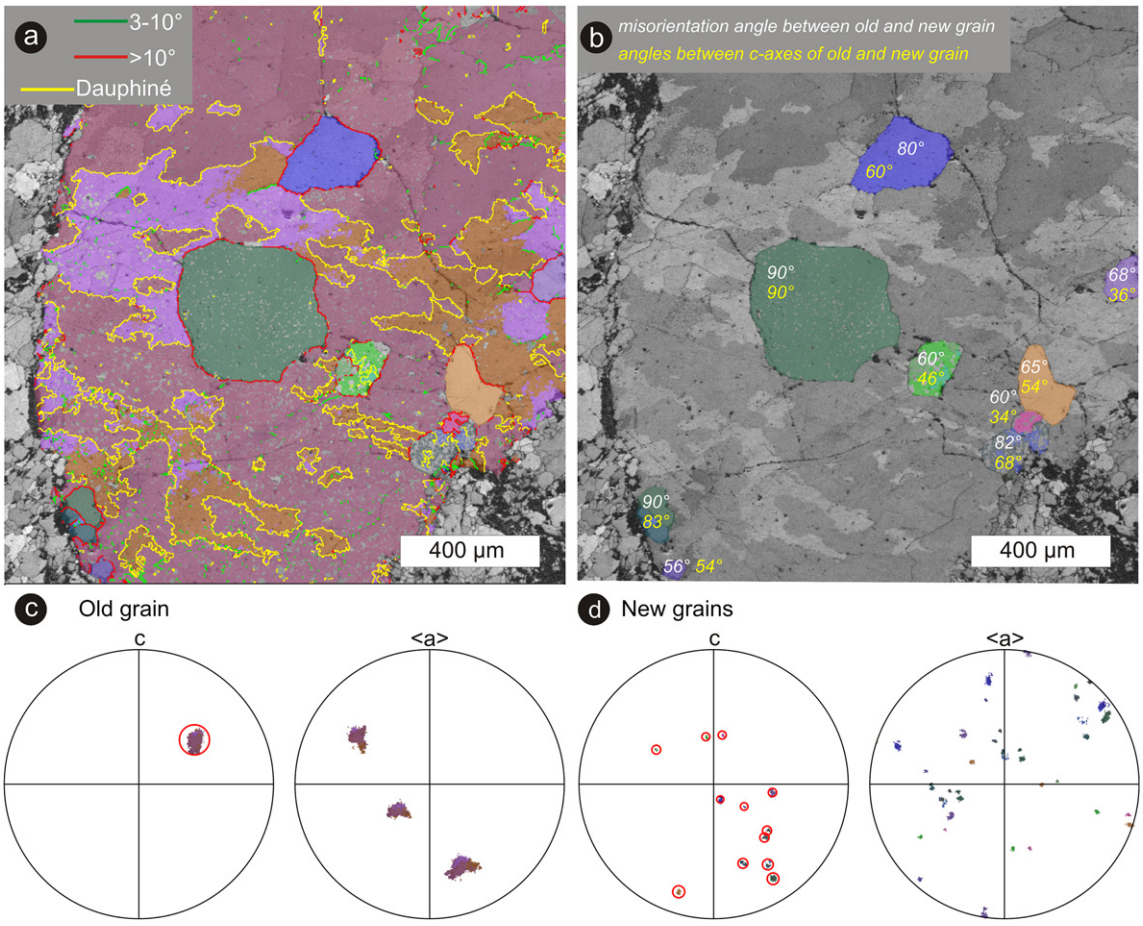

Fig. 6. EBSD map of quartz pebble shown in Fig. 3a (lower left rectangle, sample B8, step size 7 µm). (a) Orientation map of the quartz pebble; the surrounding matrix is displayed by band contrast only. Green lines represent LAGBs with misorientation angles between 3 and 10°, red lines represent HAGBs with misorientation angles >10°; Dauphiné twin boundaries are displayed by yellow lines. (b) The crystallographic orientations of new grains are colour coded, whereas the old grain and the matrix are displayed by band contrast. The numbers represent the misorientation angles between new and old grain. (c, d) Pole figures (equal angle, lower hemisphere) of *c*- and ⟨*a*⟩ axes of new grains and old grain, respectively. The red small circles visualize the variations of the *c*-axis orientations of <10° for the old grain and <3° for new grains.

of the excess geometrically necessary dislocations (GNDs) into LAGBs. Recovery in the Bali quartz pebbles is indicated by the well-ordered LAGBs and approximately isometric subgrains with 120 °C angles between the LAGBs at grain edges, observed within the old grains (Figs. 7 and 8c–e,h).

SIGBM ceased before replacement of the deformed old grains was completed. The record of an incomplete process may suggest that SIGBM was very slow and came to rest upon cooling. In this case, the variable proportion of new grains would be a consequence of subtle differences in the migration rate of the HAGBs, which can reflect differences in driving force or differences in mobility (Stöckhert and Duyster, 1999; Piazolo et al., 2006). Alternatively, the observed low dislocation density in both old and new grains, with at best a small contrast across the boundaries, suggests that migration eventually ceased due to competing static recovery within the old grains, which reduces the driving force for SIGBM (e.g. Poirier and Guillopé, 1979; Poirier, 1985).

6.2.3. Grain growth

Apart from stored strain energy, grain boundary migration can also be driven by the reduction of interfacial free energy. The process is commonly referred to as grain growth (e.g. Cotterill and Mould, 1976; Nicolas and Poirier, 1976; Atkinson, 1988; Stöckhert and Duyster, 1999; Evans et al., 2001; Jessell et al., 2003) or grain boundary area reduction (Passchier and Trouw, 2005). The driving force of SIGBM is orders of magnitude higher compared to that of grain growth. This means that grain growth can proceed only when a very low dislocation density is attained. In minerals with low anisotropy of interfacial free energy, grain growth leads to development of an energetically favourable foam microstructure, characterized by planar or simply curved grain boundaries and 120° angles at the grain edges (e.g. Cotterill and Mould, 1976).

In type 3 pebbles, such planar or smoothly curved HAGBs meeting with 120° angles at the grain edges are restricted to aggregates of new grains (Figs. 4d–f). They are neither observed between old and new grains, nor between two old grains. As such, only in quartz aggregates devoid of subgrains and characterized by a low free dislocation density on the order of 10^{11}–10^{12} m^{-2}, the grain shape developed driven by the reduction of interfacial free energy. After recovery, the migration of HAGBs between old grains or old and new grains, driven by the reduction of interfacial free energy, was probably hindered by LAGBs (Figs. 4e,f and 8c–f,h). Abundant LAGBs in old grains affect the shape of the HAGBs (Figs. 8c–f,h), which does not allow the development of a foam microstructure. The same may also hold for the other types of quartz pebbles, where – on the optical scale – the microstructures imported from the source rock are not notably modified by grain growth.

6.2.4. Fluid inclusions and fluid transport along grain boundaries

Old grains are rich in fluid inclusions, mostly arranged along healed cracks. Along grain boundaries, voids with a small dihedral angle are observed by TEM (Figs. 8c–f,h and 9e,f), similar to those

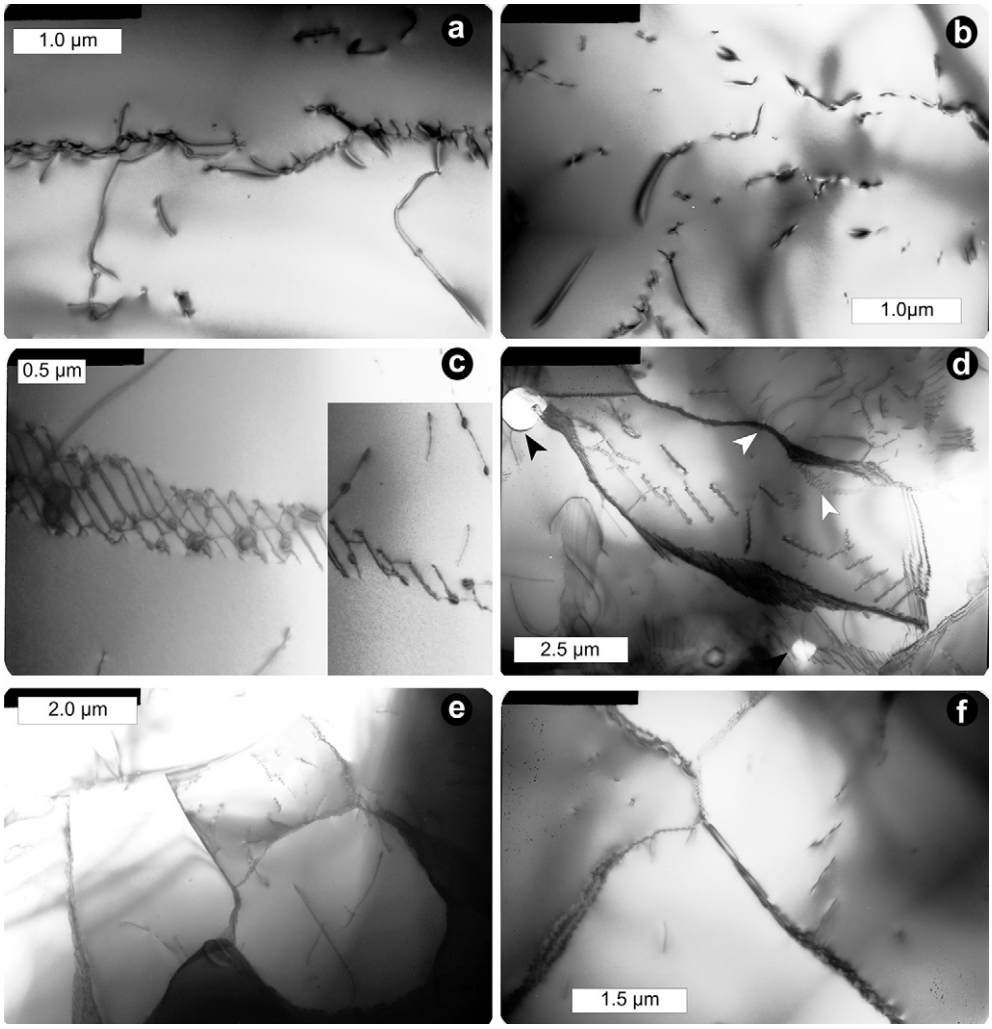

Fig. 7. TEM micrographs of defect structure within old grains (sample B8). Samples are prepared by ion milling. (a, b) Old grains show a low free dislocation density on the order of (10^{12} m^{-2}). (c) Dislocations are arranged in tilt boundaries. (d) LAGBs can be slightly curved (white arrows) and decorated by fluid inclusions (black arrows). (e, f) LAGBs bound isometric subgrains. The angle at triple junctions is commonly 120°.

described by White and White (1981). In contrast, new grains contain only few or essentially no fluid inclusions (Figs. 4a,b). This suggests that the inclusions were eliminated in the volume swept by a HAGB during recrystallization (e.g., Urai et al., 1986; Jessell et al., 2003; Schenk and Urai, 2005). According to observations reported from laboratory experiments on synthetic salt minerals, the fluid inclusions within the old grains are collected by migrating high angle grain boundaries, and are partly incorporated into the new grain (Urai et al., 1986; Drury and Urai, 1990; Schenk and Urai, 2004, 2005). Theoretical models predict that the conditions of grain boundary migration determine whether a pore will be dragged along or dropped and left within the growing crystal (Petrishcheva and Renner, 2005). Schenk and Urai (2005) observed the migration of HAGBs of bischofite *in situ*. Based on these laboratory experiments they proposed that incorporation of fluid inclusions into the recrystallizing grain occurs when the surface energy of the inclusion exceeds the dragging force of a fast migrating boundary. At slow migration rates, the content of fluid inclusions rather spreads laterally into the migrating grain boundary and becomes dragged along or drained into an external reservoir. In the type 3 quartz pebbles, there is no evidence for any significant transfer of fluid inclusions into the growing new grains. New grains are almost free of fluid inclusions, thus indicating a relative low migration velocity (Schenk and Urai, 2005). Instead, submicron-sized voids characterized by a small dihedral angle are observed along the HAGBs on the TEM scale (Figs. 8d,f,h and 9e,f). The volume of the tiny grain boundary voids is orders of magnitude smaller compared to the estimated total volume of the fluid inclusions, visible in the optical microscope in the interior of the old grains, in the area presumably swept by the migrating HAGB. This relation indicates that the major portion of the fluid collected by the migrating grain boundary must have been drained into an external reservoir during SIGBM. This fluid transport probably occurred along the grain boundary network and/or tubes along the grain edges (e.g. White and White, 1981; Watson and Brenan, 1987; Schenk and Urai, 2004, 2005; Schenk et al., 2006), as indicated by the low dihedral angle (Figs. 8c–f,h and 9c–f,h). At the given circumstances, the transport of the fluid phase along the HAGBs must have been rapid compared to the rate of SIGBM. In turn, the fluid phase has probably facilitated grain boundary migration (Urai, 1983, 1985, 1987; Mancktelow and Pennacchioni, 2004; Schenk and Urai, 2004, 2005; Schenk et al., 2006).

6.3. Geological implications

The bulk conglomerate has been deformed by dissolution-precipitation creep, most probably during Miocene metamorphism of the Plattenkalk unit, in the Talea Ori window at temperatures of c.

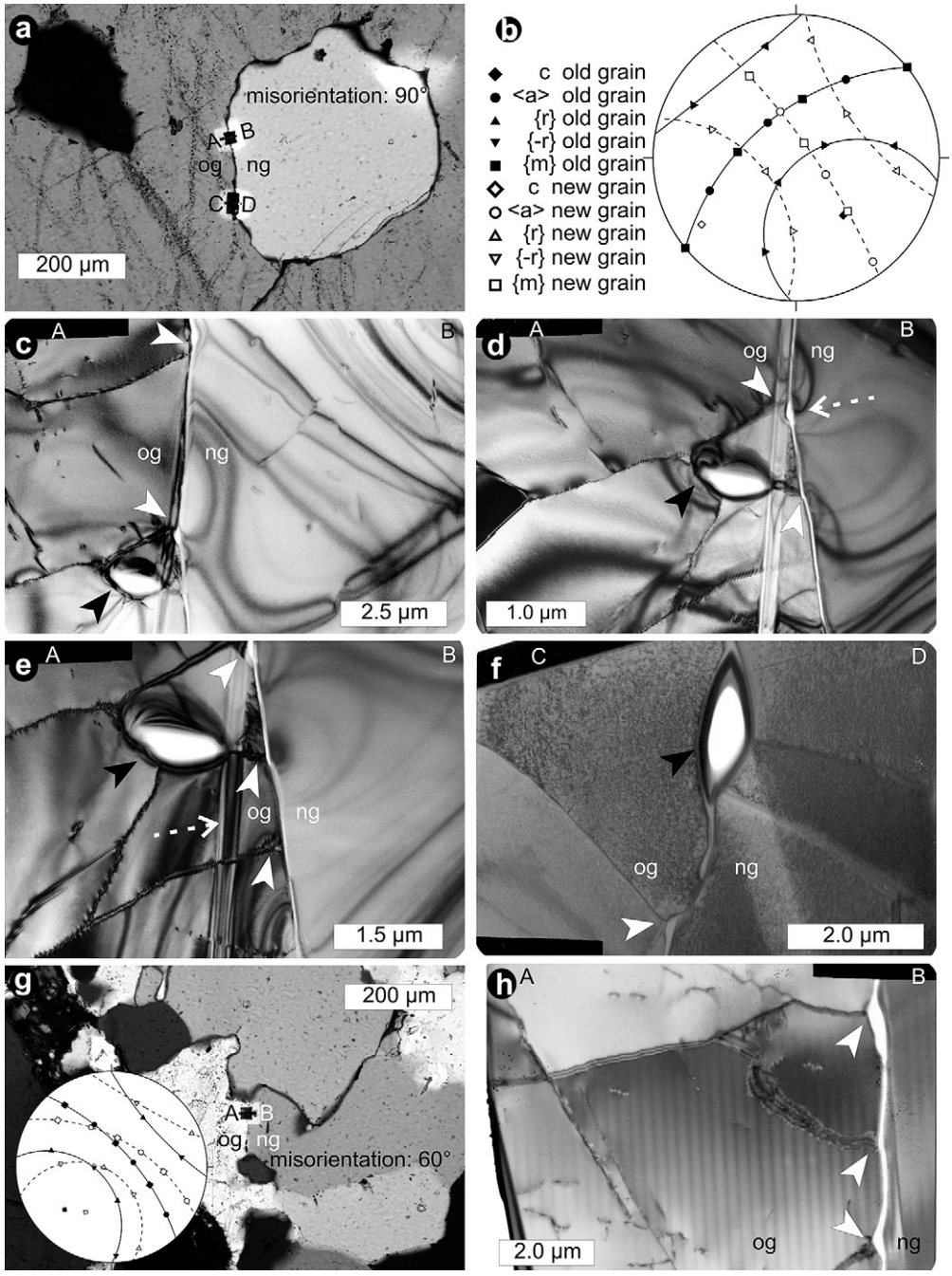

Fig. 8. Images show HAGBs between old and new grains and the effect of the LAGBs within old grains. (a) Optical micrograph (crossed polarizers) showing locations of TEM samples that cover boundaries between new and old grains (AB, CD); TEM micrographs of these samples are presented in (c–f). (b) Stereographic projection of ⟨*a*⟩ and *c*-axes and poles to {*r*}, {-*r*} and {*m*} planes in old and new grains shown in (a). The basal plane (great circle) and the 52° small circle around the *c*-axes are displayed as solid line for the old grain and as dashed line for the new grain. (c–e) TEM micrographs from sample (AB), the location is shown in (a). The boundary between the old and the new grain appears retracted by LAGBs (white arrows). A fluid inclusion is linked to LAGBs (black arrows) in the old grain. The new grain is almost free of dislocations. A fissure in the TEM sample is an artefact from preparation (dashed white arrows). (f) TEM micrograph of sample (CD), location is shown in (a). The grain boundary appears retracted by the LAGB in the old grain (white arrow). Black arrow marks fluid inclusion at the grain boundary. Quartz is strongly affected by radiation damage. (g) Optical micrograph (crossed polarizers) showing location of sample, from which a TEM micrograph is presented in (h). Stereographic projection of the crystallographic orientation of new and old grain is inserted; symbols are explained in (b). (h) TEM micrograph showing boundary between old grain with LAGBs and almost new grain almost free of dislocations. The grain boundary is retracted by the LAGBs (white arrows).

350 °C (Seidel et al., 1982; Theye, 1988; Theye et al., 1992). Deformation by dissolution-precipitation creep proceeds at a low level of differential stress (e.g. Rutter, 1976), as shown for siliciclastic metasediments in the Phyllite-Quartzite unit overlying the Plattenkalk unit in Crete (Schwarz and Stöckhert, 1996; Stöckhert et al., 1999). The microstructural diversity of all quartz pebbles in the conglomerate precludes a significant modification of the source rock microfabrics by crystal-plastic deformation. Instead, static recrystallization has occurred in the type 3 quartz pebbles. As such, differential stress during the entire metamorphic history of the conglomerate is inferred to have generally remained too low to drive crystal-plastic deformation or dislocation creep of quartz and low enough to enable static recrystallization in grains with a sufficiently high driving force.

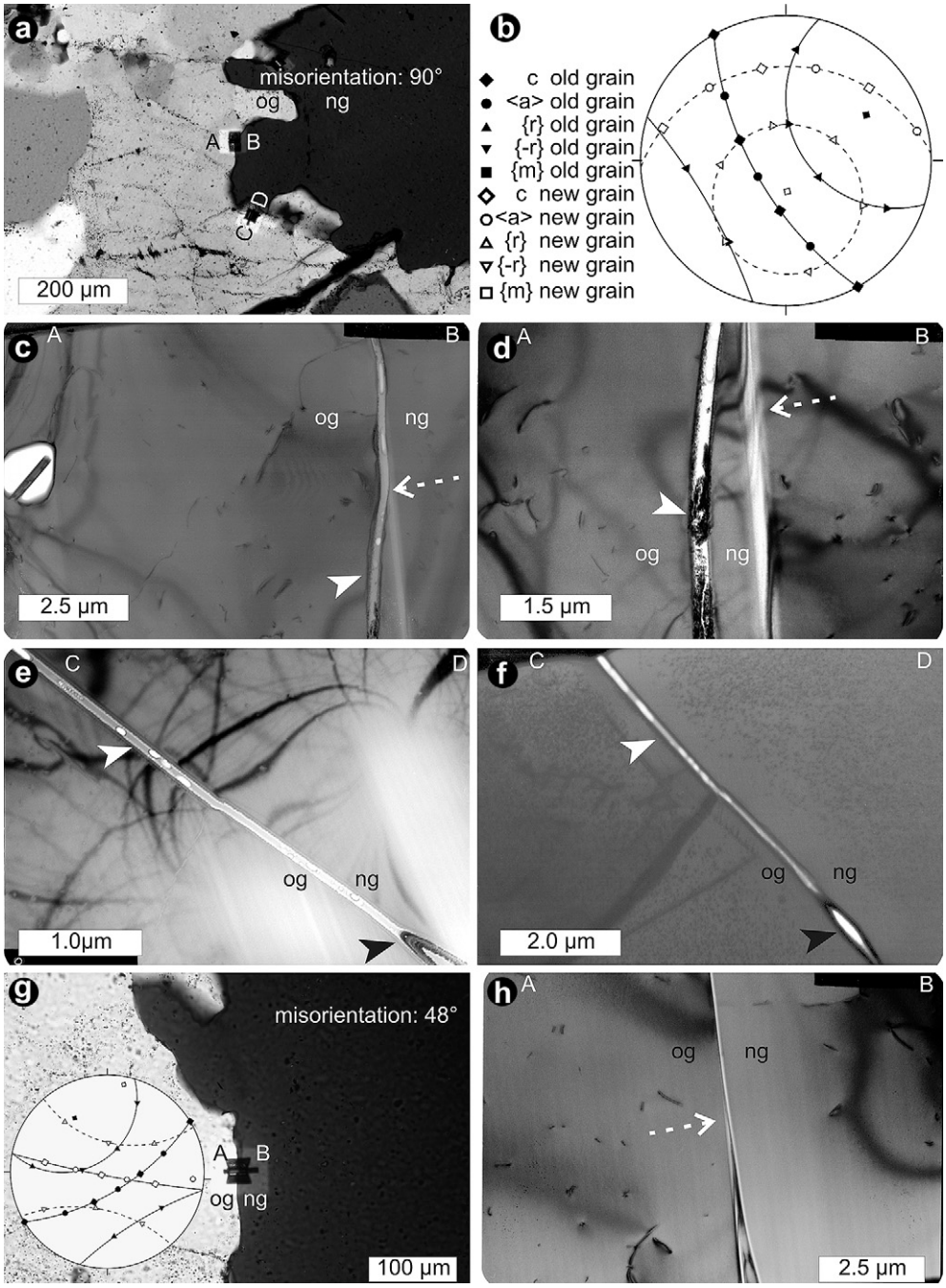

Fig. 9. Images show straight HAGBs between old and new grains. (a) Optical micrograph (crossed polarizers) showing locations of TEM samples that cover boundaries between new and old grains (AB, CD); TEM micrographs are presented in (c–f). (b) Stereographic projection of ⟨*a*⟩ and *c*-axes and poles to {*r*}, {-*r*} and {*m*} planes in old and new grains shown in (a). The basal plane (great circle) and the 52° small circle around the *c*-axes are displayed as solid line for old grain and as dashed line for new grain. (c, d) TEM micrographs from sample (AB), location is shown in (a). The dislocation density is low in both the old and the new grain. A fissure in the TEM sample is an artefact from FIB preparation (dashed white arrows). Black arrow marks a fluid inclusion in the old grain. (e, f) TEM micrographs from sample (CD), location is shown in (a). The grain boundary has a relatively shallow dip. Black arrows mark fluid inclusion at the grain boundary. (g) Optical micrograph (crossed polarizers) showing location of TEM sample from which a micrograph is presented in (h). Stereographic projection of the crystallographic orientation of new and old grain is inserted; symbols are explained in (b). (h) TEM micrograph showing a straight boundary between the old and the almost dislocation-free new grain. Dashed white arrow marks fissure in TEM sample, which is an artefact from FIB preparation.

As all quartz pebbles of the conglomerate followed the same pressure–temperature–time path and were subject to the same low level of differential stress, the wide variety of quartz microfabrics shown by the different pebbles derived from different sources is striking. Clearly, the processes proceeding at c. 350 °C in the conglomerate did not lead to a uniform microstructure. The only obvious microstructural changes are confined to the type 3 pebbles originating from vein quartz, whose microstructure suggests preceding deformation in the low-temperature plasticity field. The dislocation density imported into the sediment may have been significantly higher compared to the other pebble types, in particular those showing evidence of dynamic recrystallization. An inferred higher dislocation density in the type 3 quartz pebbles may have been the primary cause for SIGBM. This is supported by experimental results obtained by Ree and Park (1997) on octachloropropane, and by Heilbronner and Tullis (2002) on quartz. In these experiments, the

materials were statically annealed after deformation at various conditions. The microstructural modifications were more significant the higher the previously stored strain energy was. In addition, the availability of significant quantities of fluid in abundant inclusions in the type 3 quartz pebbles may have facilitated grain boundary migration.

The diversity of microstructures in the pebbles, that were all subject to the same history once joined in the conglomerate, suggests that the rate of specific microstructural processes in quartz is highly dependent on the pre-existing defect structure and probably – though poorly understood – the availability of H_2O and related defects. This sensitivity seems to be particularly effective at temperatures of c. 350 °C and low differential stress. For example, Stöckhert and Duyster (1999) reported microfabrics indicating stranded discontinuous grain growth at similar conditions.

7. Summary and conclusions

The quartz pebbles in the HP-LT metamorphic conglomerate have retained a wide spectrum of microstructures, which originated from processes of deformation, dynamic recrystallization and recovery in the source rock. In this respect, the continental crust exposed in the source area of the conglomerate was quite heterogeneous. In the present study we have focused on the type 3 quartz pebbles, which are interpreted to be derived from quartz veins. This vein quartz was inhomogeneously deformed in the low-temperature plasticity field, when still residing in the source rock. After exhumation, these quartz veins were eroded, transported as pebbles, and finally deposited in a coarse-grained clastic sediment, probably in Permian times. This conglomerate was buried at the Hellenic convergent plate boundary, deformed by dissolution-precipitation creep, and heated to moderate temperatures of c. 350 °C during HP-LT metamorphism of the Plattenkalk unit in the Miocene. At these conditions, the deformed quartz grains in type 3 pebbles underwent static recrystallization. The microstructures of other pebbles were not notably modified on the optical scale.

Based on the microstructures of the type 3 pebbles, the following is concluded:

(1) The elevated dislocation density (stored strain energy) in the old grains acquired by inhomogeneous deformation in the low-temperature plasticity regime within the source rock was retained during exhumation, transport, deposition, and re-burial of the conglomerate.
(2) New defect-free grains grew by SIGBM at the expense of the deformed old grains, driven by the reduction of stored strain energy.
(3) Fluid inclusions from the interior of the deformed old grains were eliminated and their fluid content was drained along the migrating grain boundary into an external reservoir. The transport of the fluid along the migrating grain boundaries was fast compared to the rate of migration.
(4) SIGBM eventually ceased because simultaneous static recovery in the deformed old grains progressively reduced the driving force. This is indicated by the low dislocation density that is similar in old and new grains, the well-ordered LAGBs, and the isometric subgrains now observed in the old grains.
(5) Microstructures controlled by the reduction of interfacial energy (grain growth) are only observed within aggregates of new grains, where the dislocation density was sufficiently low to allow grain boundary migration driven by interfacial free energy, not hindered by the presence of LAGBs.
(6) Static recrystallization is restricted to the vein quartz in the type 3 pebbles with a high defect density and fluid inclusion content brought into the sediment from the source rock. This observation suggests that SIGBM is highly sensitive to the dislocation microstructure generated during the preceding deformation, and perhaps also to the presence of H_2O as inclusions or water-related defects.
(7) Static recrystallization took place during HP-LT metamorphism of the conglomerate at c. 350 °C within the type 3 pebbles, while the bulk conglomerate was deformed by dissolution-precipitation creep at a level of differential stress too low to drive deformation of quartz by dislocation creep. Internally, the pebbles remained undeformed. This allowed the preservation of the wide variety of microstructures brought into the sediment.

Acknowledgements

Financial support by the Deutsche Forschungsgemeinschaft within the scope of Collaborative Research Centre 526 "Rheology of the Earth – from the upper crust into the subduction zone" is acknowledged. We are particularly grateful to Eberhard Seidel for sharing his insight into the geology of Crete with us. Constructive reviews by Sandra Piazolo and Joe White are gratefully acknowledged.

References

Atkinson, H.V., 1988. Theories of normal grain growth in pure single phase systems. Acta Metallurgica 36, 469–491.
Bachmann, R., Glodny, J., Oncken, O., Seifert, W., 2009. Abandonment of the South Penninic–Austroalpine palaeosubduction zone, Central Alps, and shift from subduction erosion to accretion; constraints from Rb/Sr geochronology. Journal of the Geological Society of London 166, 217–231.
Bestmann, M., Piazolo, S., Spiers, C.J., Prior, D.J., 2005. Microstructural evolution during initial stages of static recovery and recrystallization: new insights from in-situ heating experiments combined with electron backscatter diffraction analysis. Journal of Structural Geology 27, 447–457.
Biino, G.G., Compagnoni, R., 1992. Very-high pressure metamorphism of the Brossasco coronite metagranite, southern Dora Maira Massif, Western Alps. Schweizerische Mineralogische und Petrographische Mitteilungen 72, 347–363.
Birtel, S., Stöckhert, B., 2008. Quartz veins record earthquake-related brittle failure and short term ductile flow in the deep crust. Tectonophysics 457, 53–63.
Brady, J.B., Markley, M.J., Schumacher, J.C., Cheney, J.T., Bianiardi, G.A., 2004. Aragonite pseudomorphs in high-pressure marbles of Syros, Greece. Journal of Structural Geology 26, 3–9.
Brix, M.R., Stöckhert, B., Seidel, E., Theye, T., Thomson, S.N., Küster, M., 2002. Thermobarometric data from a fossil zircon partial annealing zone in high pressure – low temperature rocks of eastern Crete, Greece. Tectonophysics 349, 309–326.
Buntebarth, G., Voll, G., 1991. Quartz grain coarsening by collective crystallization in contact quartzites. In: Voll, G., Töpel, J., Patterson, D.R.M., Seifert, F. (Eds.), Equilibrium and Kinetics in Contact Metamorphism. The Ballachulish Igneous Complex and its Aureole. Springer Verlag, pp. 251–265.
Chatzaras, V., Xypolias, P., Doutsos, T., 2006. Exhumation of high-pressure rocks under continuous compression: a working hypothesis for the southern Hellenides (central Crete, Greece). Geological Magazine 143, 859–876.
Cotterill, P., Mould, P.R., 1976. Recrystallization and Grain Growth in Metals. Surrey University Press, London, 409 pp.
Drury, M.R., Urai, J.L., 1990. Deformation-related recrystallization processes. Tectonophysics 172, 235–253.
Durney, D.W., Ramsay, J.G., 1973. Incremental stains measured by syntectonic crystal growths. In: DeJong, K.A., Scholten, R. (Eds.), Gravity and Tectonics. John Wiley, New York, pp. 67–95.
Epting, M., Kudrass, H.-R., Leppig, U., Schäfer, A., 1972. Geologie der Talea Ori/Kreta. Neues Jahrbuch der Geologie und Paläontologie 141, 259–285.
Evans, B., Renner, J., Hirth, G., 2001. A few remarks on the kinetics of static grain growth in rocks. International Journal of Earth Sciences 90, 88–103.
Fassoulas, C., Kilias, A., Mountraks, D., 1994. Postnappe stacking extension and exhumation of high-pressure/low-temperature rocks in the island of Crete, Greece. Tectonics 13, 127–138.
FitzGerald, J.D., Etheridge, M.A., Vernon, R.H., 1983. Dynamic recrystallization in a naturally deformed albite. Textures and Microstructures 5, 219–237.
Gerya, T.V., Stöckhert, B., 2006. 2-D numerical modeling of tectonic and metamorphic histories at active continental margins. International Journal of Earth Sciences 95, 250–274.
Gerya, T.V., Stöckhert, B., Perchuk, A.L., 2002. Exhumation rates of high-pressure metamorphic rocks in a subduction channel: a numerical simulation. Tectonics 21, 1056. doi:10.1029/2002TC001406.

Guillopé, M., Poirier, J.P., 1979. Dynamic recrystallization during creep of single crystalline halite: an experimental study. Journal of Geophysical Research 84, 5557–5567.
Haessner, F., Hofmann, S., 1978. Migration of high angle grain boundaries. In: Haessner, F. (Ed.), Recrystallization of Metallic Materials. Riederer, Stuttgart, pp. 63–95.
Hall, R., Audley-Charles, M.G., 1983. The structure and regional significance of the Talea Ori, Crete. Journal of Structural Geology 5, 167–179.
Heilbronner, R., Tullis, J., 2002. The effect of static annealing on microstructures and crystallographic preferred orientations of quartzites experimentally deformed in axial compression and shear. In: de Meer, S., Drury, M.R., de Bresser, J.H.P., Pennock, G.M. (Eds.), Deformation Mechanisms, Rheology and Tectonics: Current Status and Future Perspectives. Geological Society, vol. 200. Special Publications, London, pp. 191–218.
Hobbs, B.E., 1968. Recrystallisation of single crystals of quartz. Tectonophysics 6, 353–401.
Humphreys, F.J., Hatherly, M., 2004. Recrystallization and Related Annealing Phenomena, second ed. Pergamon, Oxford.
Jessell, M.W., 1986. Grain boundary migration and fabric development in experimentally deformed octachloropropane. Journal of Structural Geology 8, 527–542.
Jessell, M.W., Kostenko, O., Jamtveit, B., 2003. The preservation potential of microstructures during static grain growth. Journal of Metamorphic Geology 21, 481–491.
Jolivet, L., Goffé, B., Monié, P., Truffert-Luxey, C., Patriat, M., Bonneau, M., 1996. Miocene detachment in Crete and exhumation P-T-t paths of high-pressure metamorphic rocks. Tectonics 15, 1129–1153.
Karato, S.-I., 2008. Deformation of Earth Materials. University Press, Cambridge, pp. 463.
Kilias, A., Fassoulas, C., Mountrakis, D., 1994. Tertiary extension of continental crust and uplift of Psiloritis metamorphic core complex in the central part of the Hellenic Arc (Crete, Greece). Geologische Rundschau 83, 417–430.
Knipe, R.J., 1989. Deformation mechanisms m recognition from natural tectonites. Journal of Structural Geology 11, 127–146.
König, H., Kuss, S.E., 1980. Neue Daten zur Biostratigraphie des permotriadischen Autochthons der Insel Kreta (Griechenland). Neues Jahrbuch für Geologie und Paläontologie. Monatshefte 1980, 525–540.
Krahl, J., Richter, D., Förster, O., Kozur, H., Hall, R., 1988. Zur Stellung der Talea Ori im Bau des kretischen Deckenstapels (Griechenland). Zeitschrift der Deutschen Geologischen Gesellschaft 139, 191–227.
Küster, M., Stöckhert, B., 1997. Density changes of fluid inclusions in high-pressure low-temperature metamorphic rocks from Crete: a thermobarometric approach based on the creep strength of the host minerals. Lithos 41, 151–167.
Lenze, A., Stöckhert, B., 2007. Microfabrics of UHP metamorphic granites in the Dora Maira Massif, western Alps – no evidence of deformation at great depth. Journal of Metamorphic Geology 25, 461–475.
Lenze, A., Stöckhert, B., 2008. Microfabrics of quartz formed from coesite (Dora Maira Massif, Western Alps). European Journal of Mineralogy 20, 811–826.
Mancktelow, N.S., Pennacchioni, G., 2004. The influence of grain boundary fluids on the microstructure of quartz-feldspar mylonites. Journal of Structural Geology 26, 47–69.
Masuda, T., Morikawa, T., Nakayama, Y., Suzuki, S., 1997. Grain-boundary migration of quartz during annealing experiments at high temperatures and pressures, with implications for metamorphic geology. Journal of Metamorphic Geology 15, 311–322.
Nicolas, A., Poirier, J.P., 1976. Crystalline Plasticity and Solid State Flow in Metamorphic Rocks. John Wiley & Sons, New York.
Nüchter, J.A., Stöckhert, B., 2008. Coupled stress and pore fluid pressure changes in the middle crust – the vein record of coseismic loading and postseismic stress relaxation. Tectonics 27, TC1007. doi:10.1029/2007TC002180.
Otani, M., Wallis, S., 2006. Quartz lattice preferred orientation patterns and static recrystallization: natural examples from the Ryoke belt. Japan. Geology 34, 561–564.
Passchier, C.W., Trouw, R.A.J., 2005. Microtectonics, second ed. Springer Verlag, Berlin.
Petrishcheva, E., Renner, J., 2005. Two-dimensional analysis of pore drag and drop. Acta Materialia 53, 2793–2803.
Piazolo, S., Prior, D.J., Holness, M.D., 2005. The use of combined cathodoluminescence and EBSD analysis: a case study investigating grain boundary migration mechanisms in quartz. Journal of Microscopy 217, 152–161.
Piazolo, S., Bestmann, M., Prior, D.J., Spiers, C.J., 2006. Temperature dependent grain boundary migration in deformed-then-annealed material: observations from experimentally deformed synthetic rocksalt. Tectonophysics 427, 55–71.
Platt, J.P., 1986. Dynamics of orogenic wedges and the uplift of high-pressure metamorphic rocks. Geological Society of America Bulletin 97, 1037–1053.
Platt, J.P., 1993. Exhumation of high-pressure rocks: a review of concepts and processes. Terra Nova 5, 119–133.
Poirier, J.-P., 1985. Creep of Crystals – High Temperature Deformation Processes in Metals, Ceramics and Minerals. Cambridge University Press, Cambridge.
Poirier, J.P., Guillopé, M., 1979. Deformation-induced recrystallisation of minerals. Bulletin de Minéralogie 102, 67–74.
Rahl, J.M., Anderson, K.M., Brandon, M.T., Fassoulas, C., 2005. Raman spectroscopic carbonaceous material thermometry of low-grade metamorphic rocks: calibration and application to tectonic exhumation in Crete, Greece. Earth and Planetary Science Letters 240, 339–354.
Ree, J.-H., Park, Y., 1997. Static recovery and recrystallization microstructures in sheared octachloropropane. Journal of Structural Geology 19, 1521–1526.
Renner, J., Stöckhert, B., Zerbian, A., Röller, K., Rummel, F., 2001. An experimental study into the rheology of synthetic polycrystalline coesite aggregates. Journal of Geophysical Research 106, 19,411–19,429.
Richter, D., Kopp, K.O., 1983. Zur Tektonik der untersten geologischen Stockwerke auf Kreta. Neues Jahrbuch für Geologie und Paläontologie. Monatshefte 1983, 27–46.
Ring, U., Brandon, M.T., Willett, S.D., Lister, G.S., 1999. Exhumation processes. In: Ring, U., Brandon, M.T., Willett, S.D., Lister, G.S., Willet, S.D. (Eds.), Exhumation Processes: Normal Faulting, Ductile Flow and Erosion. Geological Society, vol. 154. Special Publication, London, pp. 1–27.
Rutter, E.H., 1976. The kinetics of rock deformation by pressure solution. Philosophical Transactions of the Royal Society of London. Series A 283, 203–219.
Schenk, O., Urai, J.L., 2004. Microstructural evolution and grain boundary structure during static recrystallization in synthetic polycrystals of sodium chloride containing saturated brine. Contributions to Mineralogy and Petrology 146, 671–682.
Schenk, O., Urai, J.L., 2005. The migration of fluid-filled grain boundaries in recrystallizing synthetic bischofite: first results of in-situ high-pressure, high-temperature deformation experiments in transmitted light. Journal of Metamorphic Geology 23, 695–709.
Schenk, O., Urai, J.L., Piazolo, S., 2006. Structure of grain boundaries in wet, synthetic polycrystalline, statically recrystallizing halite – evidence from cryo-SEM observations. Geofluids 6, 93–104.
Schertel, H.-P., Schreyer, W., Chopin, C., 1991. The pyrope-coesite rocks and their country rocks at Parigi, Dora Maira Massif, Western Alps: detailed petrography, mineral chemistry and PT-path. Contributions to Mineralogy and Petrology 108, 1–21.
Schwarz, S., Stöckhert, B., 1996. Pressure solution in siliciclastic HP-LT metamorphic rocks – constraints on the state of stress in deep levels of accretionary complexes. Tectonophysics 255, 203–209.
Seidel, E., Kreuer, H., Wilhelm, H., 1982. A late oligocene/early micocene high pressure belt in the external Hellenides. Geologisches Jahrbuch E32, 165–206.
Seidel, M., Seidel, E., Stöckhert, B., 2007. Tectono-sedimentary evolution of lower to middle Miocene half-graben basins related to an extensional detachment fault (western Crete, Greece). Terra Nova 19, 39–47.
Stipp, M., Kunze, K., 2008. Dynamic recrystallization near the brittle-plastic transition in naturally and experimentally deformed quartz aggregates. Tectonophysics 448, 77–97.
Stipp, M., Stünitz, H., Heilbronner, R., Schmid, S.M., 2002. The eastern Tonale fault zone: a "natural laboratory" for crystal plastic deformation of quartz over a temperature range from 250 ° to 700 °C. Journal of Structural Geology 24, 1861–1884.
Stöckhert, B., 2002. Stress and deformation in subduction zones: insight from the record of exhumed metamorphic rocks. In: De Meer, D., Drury, M.R., De Bresser, J.H.P., Pennock, G.M. (Eds.), Deformation Mechanisms, Rheology and Tectonics: Current Status and Future Perspectives. Geological Society of London. Special Publication, London, pp. 255–274.
Stöckhert, B., Duyster, J., 1999. Discontinuous grain growth in recrystallised vein quartz – implications for grain boundary structure, grain boundary mobility, crystallographic preferred orientation, and stress history. Journal of Structural Geology 21, 1477–1490.
Stöckhert, B., Wachmann, M., Küster, M., Bimmermann, S., 1999. Low effective viscosity during high pressure metamorphism due to dissolution precipitation creep: the record of HP-LT metamorphic carbonates and siliciclastic rocks from Crete. Tectonophysics 303, 299–319.
Theye, T., 1988. Aufsteigende Hochdruckmetamorphose in Sedimenten der Phyllit-Quarzit-Einheit Kretas und des Peleponnes. Dissertation, Technische Universität Carolo-Wilhelmina zu Braunschweig.
Theye, T., Seidel, E., 1991. Petrology of low-grade high-pressure metapelites from the External Hellenides (Crete, Peleponnese). A case study with attention to sodic minerals. European Journal of Mineralogy 3, 343–366.
Theye, T., Seidel, E., Vidal, O., 1992. Carpholite, sudoite, and chloritoid in low-grade high-pressure metapelites from Crete and the Peleponnese, Greece. European Journal of Mineralogy 4, 487–507.
Thomson, S.N., Stöckhert, B., Brix, M.R., 1998. Thermochronology of the high-pressure metamorphic rocks of Crete, Greece: implications for the speed of tectonic processes. Geology 26, 259–262.
Thomson, S.N., Stöckhert, B., Brix, M.R., 1999. Miocene high-pressure metamorphic rocks of Crete, Greece: rapid exhumation by buoyant escape. In: Ring, U., Brandon, M.T., Lister, G.S., Willett, S.D. (Eds.), Exhumation Processes: Normal Faulting, Ductile Flow and Erosion. Geological Society, vol. 154. Special Publications, London, pp. 87–107.
Trepmann, C., Stöckhert, B., 2003. Quartz microstructures developed during non-steady state plastic flow at rapidly decaying stress and strain rate. Journal of Structural Geology 25, 2035–2051.
Trepmann, C., Stöckhert, B., Dorner, D., Hamidzadeh Moghadam, R., Küster, M., Röller, K., 2007. Simulating coseismic deformation of quartz in the middle crust and fabric evolution during postseismic stress relaxation – an experimental study. Tectonophysics 442, 83–104.
Urai, J.L., 1983. Water assisted dynamic recrystallization and weakening in polycrystalline bischofite. Tectonophysics 96, 125–157.
Urai, J.L., 1985. Water-enhanced dynamic recrystallization and solution transfer in experimentally deformed carnallite. Tectonophysics 120, 285–317.
Urai, J.L., 1987. Development of microstructure during deformation of carnallite and bischofite in transmitted light. Tectonophysics 135, 251–263.
Urai, J.L., Means, W.D., Lister, G.S., 1986. Dynamic recrystallization of minerals. Geophysical Monograph 36, 161–199.

Vernon, R.H., 1981. Optical microstructure of partly recrystallized calcite in some naturally deformed marbles. Tectonophysics 78, 601–612.
Watson, E.B., Brenan, J.M., 1987. Fluids in the lithosphere, 1. Experimentally-determined wetting characteristics of CO2–H2O fluids and their implication for fluid transport, host-rock physical properties, and fluid inclusion formation. Earth and Planetary Science Letters 85, 497–515.
White, S., 1977. Geological significance of recovery and recrystallization processes in quartz. Tectonophysics 39, 143–170.
White, J.C., 1982. Quartz deformation and the recognition of recrystallization regimes in the Flinton Group conlomerates, Ontario. Canadian Journal of Earth Sciences 19, 81–93.
White, J.C., Mawer, C.K., 1988. Dynamic recrystallization and associated exsolution in perthites: evidence of deep crustal thrusting. Journal of Geophysical Research 93, 325–337.
White, J.C., White, S.H., 1981. On the structure of grain boundaries in tectonites. Tectonophysics 78, 613–628.
Wirth, R., 1985. The influence of the low high quartz transformation on recrystallization and grain growth during contact-metamorphism (Traversella intrusion, north Italy). Tectonophysics 120, 107–117.
Wirth, R., 2004. Focused Ion Beam (FIB): a novel technology for advanced application of micro- and nanoanalysis in geosciences and applied mineralogy. European Journal of Mineralogy 16, 863–876.